ACS Macro Letters

Letter

pubs.acs.org/macroletters

Poly(cyclohexylethylene)-*block*-poly(ethylene oxide) Block Polymers for Metal Oxide Templating

Morgan W. Schulze,[†] Christophe Sinturel,[‡,§] and Marc A. Hillmyer*[,‡]

[†]Department of Chemical Engineering and Materials Science and [‡]Department of Chemistry, University of Minnesota, Minneapolis, Minnesota 55455-0431, United States

[§]ICMN, UMR 7374 - CNRS/Université d'Orléans, 1b rue de la Férollerie, 45071 Orléans, France

Supporting Information

ABSTRACT: A series of poly(cyclohexylethylene)-*block*-poly(ethylene oxide) (CEO) diblock copolymers were synthesized through tandem anionic polymerizations and heterogeneous catalytic hydrogenation. Solvent-annealed CEO diblock films were used to template dense arrays of inorganic oxide nanodots via simple spin coating of an inorganic precursor solution atop the ordered film. The substantial chemical dissimilarity of the two blocks enables (i) selective inclusion of the inorganic precursor within the PEO domain and (ii) the formation of exceptionally small feature sizes due to a relatively large interaction parameter estimated from mean-field analysis of the order−disorder transition temperatures of compositionally symmetric samples. UV/ozone treatment following incorporation produces an ordered arrangement of oxide nanodots and simultaneously removes the block polymer template. Herein, we report the smallest particles (6 ± 1 nm) templated from a selective precursor insertion method to date using a block polymer scaffold.

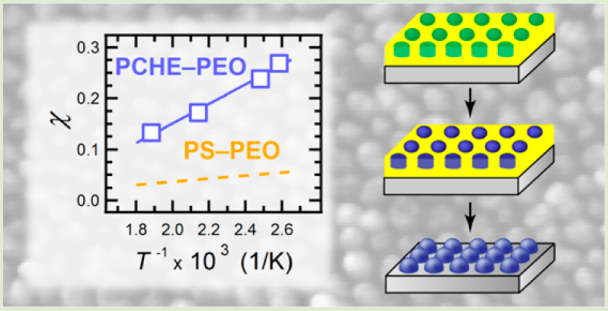

Dense arrays of nanostructured metal oxides offer diverse functionality for a broad range of technologies, including optoelectronics,[1,2] magnetic storage,[3,4] and photocatalysis.[5,6] Their utility motivates the investigation of tractable, low-cost strategies to produce precision nanostructure arrays. Block copolymer (BCP) nanolithography has emerged as a powerful bottom-up patterning technique in which synthetically controllable variables, such as the overall degree of polymerization (N), the block incompatibility (χ), and the composition (f), dictate the morphology and length scale of the patterned structures.[7−9] The ability of block polymers to produce well-defined features for ultrahigh density arrays is dictated by the segregation strength (χN).[43] At reduced values of N needed for very small feature sizes, the diffuse interfaces of weakly segregated block polymers can result in significant line edge roughness, an issue exacerbated by the limited etch contrast of typical organic blocks.[7−10]

The need to simultaneously increase χ and the block etch contrast has motivated the introduction of segments containing inorganic elements.[10] Although often high-χ materials, inorganic−organic diblocks can be difficult to prepare and have limited versatility in terms of the product metal oxide. New high-χ diblocks reliant on "etchless" technology are attractive alternatives to inorganic−organic block polymers. In the etchless approach, selective inclusion of inorganic additives into a single domain occurs upon exposure of a self-assembled film to a dilute solution of inorganic precursors. Subsequent UV/ozone, thermal, or plasma treatment of the film removes the organic polymer scaffold and generates a metal oxide in situ, thereby readily replicating the structure of the initial template. Previous demonstrations of this selective inclusion technique have relied on the combination of a hydrophobic block, typically polystyrene (PS), and a more polar metallophilic block such as poly(vinylpyridine) (PVP)[11−15] or poly(ethylene oxide) (PEO).[16−20] Although these polar candidates offer exceptional flexibility and imbibe both sol−gel reactants and metal ions, their relatively low incompatibility with the hydrophobic blocks typically used places a lower limit on the accessible particle dimensions.

To enable ultrasmall etchless particle formation, the ideal block polymer would combine two highly incompatible low molar mass segments distinguished by marked differences in hydrophobicity and hydro(metallo)philicity. Although it has been shown that high-χ, low-T_g polyolefin−PEO block polymers can adopt domain sizes below 10 nm at synthetically accessible molar masses, their mechanical and thermal properties are likely inadequate for nanopatterning purposes.[21−23] Poly(cyclohexylethylene) (PCHE), however, is a simple polymeric hydrocarbon that is attractive due to its exceptionally high glass transition temperature.[24,25] In this study, we prepared a new highly incompatible block polymer system, poly(cyclohexylethylene)-*block*-poly(ethylene oxide) (CEO), and

Received: July 6, 2015
Accepted: August 25, 2015
Published: September 1, 2015

DOI: 10.1021/acsmacrolett.5b00458
ACS Macro Lett. 2015, 4, 1027−1032

utilized it in thin films to template metal oxides of exceptionally small dimensions.

The route to CEO materials shown in Scheme 1 starts with functionalized polystyrene precursors synthesized by end-capping polystyrllithium anions with ethylene oxide to give hydroxyl-terminated polystyrene (PSOH). The relatively low degrees of polymerization (DP) enabled precise ^{1}H NMR spectroscopy determination of the molar mass and end-capping efficiency from the molar ratio of the *sec*-butyllithium initiator fragment ($-CH_3$, 0.7 ppm) to the aromatic backbone (6.3−7.1 ppm) and ethoxy end group ($-CH_2-OH$, 3.3 ppm), respectively (Figure S1). Using $Pd/CaCO_3$ at 120 °C for the catalytic hydrogenation of PSOH,[26,27] we found that no residual aromatic resonances remained in the ^{1}H NMR spectra after 48 h (conversion >99%), and quantitative retention of the hydroxyl functionality was achieved (i.e., DP(PSOH)/DP(PCHEOH) ≈ 1). The narrow molar mass distributions of the hydrogenated PCHEOH products also indicated saturation without significant side reaction (Figure S2). Table S1 summarizes the molecular characteristics of the PCHEOH samples and their corresponding PSOH precursors. The molar masses of the PCHEOH samples are reported as the hydrogenous equivalent molar mass of the PSOH precursor and account for end groups. Even though the PCHE precursors are of very low molar mass, the T_g values are still relatively high (75−118 °C) (Figures S3 and S4).

Potassium naphthalenide was used to convert macromolecular PCHEOH alcohols into potassium alkoxides for EO initiation.[21] Block polymer compositions were determined from the ^{1}H NMR spectra of the CEO block polymers (Figure S5) and spanned a broad range of volume fractions ($0.17 \leq f_{PEO} \leq 0.82$) (see Table 1 and Table S2). SEC analysis (Figures S6 and S7) shows the shift to lower elution volumes upon formation of diblocks. From the overlay of block polymer and precursor traces, some unreacted starting material is evident implying, in fact, some minor loss of hydroxyl functionality in the hydrogenation step.[26,27] However, peak-fitting analysis generally indicated approximately 3−5 wt % homopolymer where contamination was evident; this low level of homopolymer contamination was neglected in subsequent analysis.

In general, the use of fully saturated PCHE hydrocarbons as initiators for the polymerization of EO produces block polymer amphiphiles with exceptional thermal stability as determined by thermal gravimetric analysis (TGA) ($T_{d,CEO}$ = 349 °C, Figure S8). Previous reports on polyalkane−poly(ethylene oxide)s have shown that crystalline breakout results when the poly(ethylene oxide) microdomains are surrounded by a rubbery matrix.[28] Although by differential scanning calorimetry (DSC) the EO blocks retain high crystallinity (41 wt %) at molar masses as low as 1.5 kg/mol (Figure S9), PCHE vitrification above T_c leads to hard nanoconfinement and preserves the amorphous melt morphology at low temperature in all samples.[29,30]

Dynamic mechanical spectroscopy (DMS) experiments performed by slowly heating from the ordered state were used to determine the order−disorder transition (ODT) temperature, T_{ODT}, identified as a discontinuous drop in the dynamic elastic modulus (G') resulting in a liquid-like response (Figure 1). Weak latent heats associated with the ODT and observable in the DSC thermograms of several CEO block polymers are consistent with T_{ODT} determined by DMS (Figure S9, onset temperatures are indicated in parentheses in Table 1).[31] Moreover, the ODT was verified by small-angle X-ray scattering experiments (Figure S10); the inset of Figure 1 shows a representative transition for N = 44 upon cooling at T ≈ 130 °C in close agreement with T_{ODT} determined by DMS. The DMS data for the N = 61 and 79 samples suggest the presence of an order−order transition (OOT) prior to the ODT even though these samples are compositionally symmetric (Table 1).

In the determination of $\chi_{CEO}(T)$, we have utilized the mean field value of $(\chi N)_{ODT}$ = 10.5, thus knowing N the value of χ can be estimated at a given ODT temperature. Rigorously, this applies only to compositionally (f = 1/2) and conformationally symmetric (i.e., equal statistical segment lengths $b_a = b_b$) and monodisperse ($Đ$ = 1.0) block polymers in the limit of infinitely large N.[31,32] However, these criteria are typically relaxed in the experimental analysis of real block polymers so that estimates of

Scheme 1. Synthesis of Poly(cyclohexylethylene)-*block*-poly(ethylene oxide) (CEO)

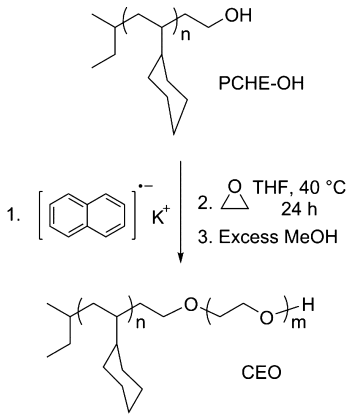

Table 1. Molecular Characteristics of Synthesized PCHE−PEO Diblock Copolymers

entry[a]	precursor[b]	$M_{n,PEO}$ (kg/mol)[c]	$Đ$[d]	f_{PEO}[e]	N[f]	T_{ODT}[g] (°C)
CEO (2.7, 0.55)	PCHEOH (1.2)	1.5	1.14	0.55	39	114 (114)
CEO (3.1, 0.51)	PCHEOH (1.5)	1.6	1.12	0.51	44	130 (133)
CEO (4.3, 0.50)	PCHEOH (2.0)	2.2	1.07	0.50	61	194 (195)
CEO (5.6, 0.51)	PCHEOH (2.6)	2.9	1.09	0.51	79	258
CEO (5.9, 0.42)	PCHEOH (3.2)	2.6	1.10	0.42	85	240

[a]CEO (X, Y) corresponds to PCHE−PEO of total molecular weight X, including the *s*-butyllithium end-group, and f_{PEO} (Y). [b]See Table S1. [c]Number-average molar mass of PEO was calculated from ^{1}H NMR spectra. [d]Determined using LS-SEC. [e]Calculated volume fraction of PEO using bulk densities of PCHE (0.92 g/cm^3) and PEO (1.06 g/cm^3) at 140 °C. [f]Number-average degree of polymerization calculated using a reference volume of 118 Å^3. [g]T_{ODT} was determined by dynamic mechanical spectroscopy (DMS). Values indicated in parentheses were determined from differential scanning calorimetry.

DOI: 10.1021/acsmacrolett.5b00458
ACS Macro Lett. 2015, 4, 1027−1032

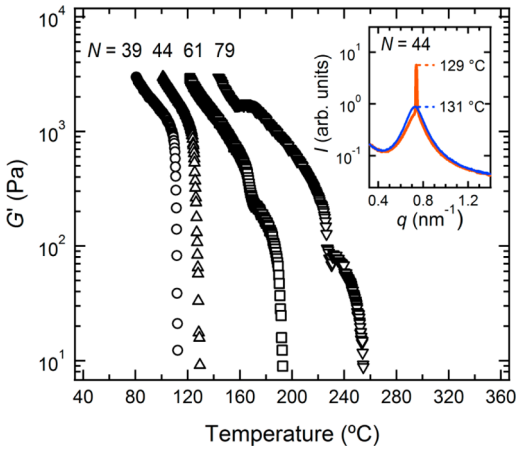

Figure 1. Temperature dependence of the low-frequency dynamic elastic shear modulus (G') for four compositionally symmetric samples and the determination of T_{ODT}. Samples were loaded onto a parallel plate fixture, heated above the order−disorder transition in an N_2 atmosphere, and subsequently quenched and annealed at reduced temperature for 1 h prior to measurement. The data were then obtained at a ramp rate of 1 °C/min under relatively small strain (≤1.2%) and a frequency of 1 rad/s. The inset shows the transition from a disordered-to-ordered phase upon cooling via SAXS for $N = 44$ at $T \approx 130$ °C.

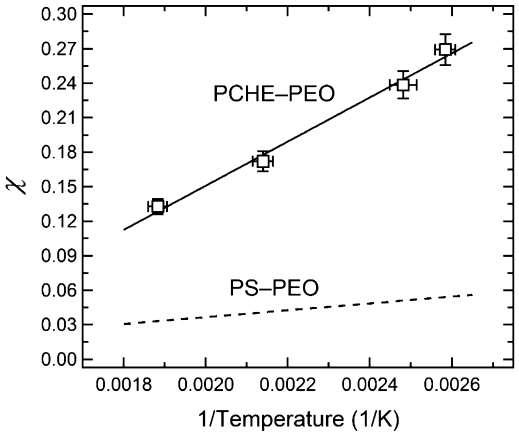

Figure 2. $\chi(T)$ for compositionally symmetric diblock copolymers determined using the first four entries of Table 1. The interaction parameter of PS−PEO is provided by Cochran et al. using the same method applied here.[37] Data are reported using an equivalent monomer reference volume (ν_o = 118 Å^3).

χ can be made for comparative purposes. Within self-consistent field theory (SCFT), $(\chi N)_{ODT}$ for conformationally symmetric, monodisperse samples is approximately equal to 10.5 at the moderately asymmetric compositions $f = 0.45$ or 0.55.[33,34] Similarly, extreme conformational asymmetry ($b_a/b_b = 2$) accounts for an increase in $(\chi N)_{ODT}$ by less than 5% at $f = 0.50$.[34] For real block polymers with $Đ > 1$, calculated values of $(\chi N)_{ODT}$ also do not vary appreciably provided $Đ$ is not too large.[35,36] SCFT suggests only small Gibbs free energy differences between different ordered states at the same composition near the ODT. Thus, we posit that consistent estimation of χ by applying $(\chi N)_{ODT} = 10.5$ for CEO diblock polymers that are approximately symmetric ($f = 0.5 \pm 0.05$), and of low dispersity ($Đ < 1.2$), will allow for useful comparisons recognizing errors associated with the differences between real systems and mean field predictions. We note in our analysis that all samples exhibit the same apparent morphology in the vicinity of the ODT by SAXS (Figure S10), and the OOT prior to the ODT for $N = 61$ and 79 (both nearly symmetric) occurs at near equivalent values of χN given the estimate of χ we make below. Definitive morphological identification of the phases present in these materials is ongoing.

Using the values of T_{ODT} for the four symmetric samples in Table 1, applying $(\chi N)_{ODT} = 10.5$ and $\chi = \alpha/T + \beta$ we determined the temperature dependence of χ_{CEO} as

$$\chi_{CEO}^{118} = \frac{(192 \pm 13)}{T} - (0.23 \pm 0.03) \quad (1)$$

We have therefore developed a highly segregated block polymer to direct the nanoscale structure of inorganic materials through selective metal inclusion in the PEO domains (Figure 2). DMS and SAXS experiments show that one sample in particular CEO (5.9, 0.42) produces a hexagonally packed cylindrical microstructure that transitions to the gyroid phase before disorder (Figure S11), similar to related systems.[28] Bulk SAXS measurement of the hexagonal unit cell spacing reveals 10 nm diameter features and a 15 nm center-to-center distance at room temperature. As-cast CEO films give an ill-defined structure and display a mixed orientation of domains with respect to the substrate surface. Furthermore, disparate interfacial energies of each block-interface combination promote a parallel domain orientation upon thermal annealing (Figure S12a).

Solvent vapor annealing can simultaneously induce chain mobility and circumvent preferential surface interactions. As solvent evaporates from the swollen film, a rapid evaporation front perpendicular to the plane of the substrate can nucleate a potentially nonequilibrium orientation of the ordered phase.[38,39] Here, a 5 min exposure of CEO films to a 50/50 (v/v) mixture of cyclohexane/THF produced a hexagonal arrangement of features perpendicular to the free surface (Figure 3a and Figure S13a). These data contrast the parallel orientation of PEO cylinders observed after either thermal annealing or solvent annealing with other nonselective solvents (see Figure S12b); however, we note that this solvent mixture produced a parallel orientation for lamellar block polymer films. AFM measurements of these features, which may be spheres or perpendicular cylinders, yield a center-to-center distance estimate of 22 ± 3 nm and a diameter of 13 ± 3 nm, a significant increase in feature size relative to those observed in the bulk. Cushen et al.[40,41] previously showed similar domain enlargement (~30%) following selective solvent vapor annealing, attributable to (i) an effective increase in the segregation strength between the domains and (ii) an effective increase in the occupied volume of the swollen block at appreciable concentrations. In our case, annealing with a single strongly preferential solvent (cyclohexane) resulted in an overall domain increase of ~70% under comparable exposure times. We suspect that selective inclusion of cyclohexane into the PCHE domains increases χ_{eff} and induces chain stretching, and this state is then trapped during rapid evaporation. Hence, the miscible, binary mixture of THF and cyclohexane significantly mitigates domain enlargement. The result may imply that THF, the more volatile component of the nonideal mixture,[42] significantly reduces the vapor pressure of cyclohexane relative to pure solvent, resulting in a less swollen PCHE domain. Second, the addition of THF, a nonselective solvent enriched in the vapor phase, may screen block−block

DOI: 10.1021/acsmacrolett.5b00458
ACS Macro Lett. 2015, 4, 1027−1032

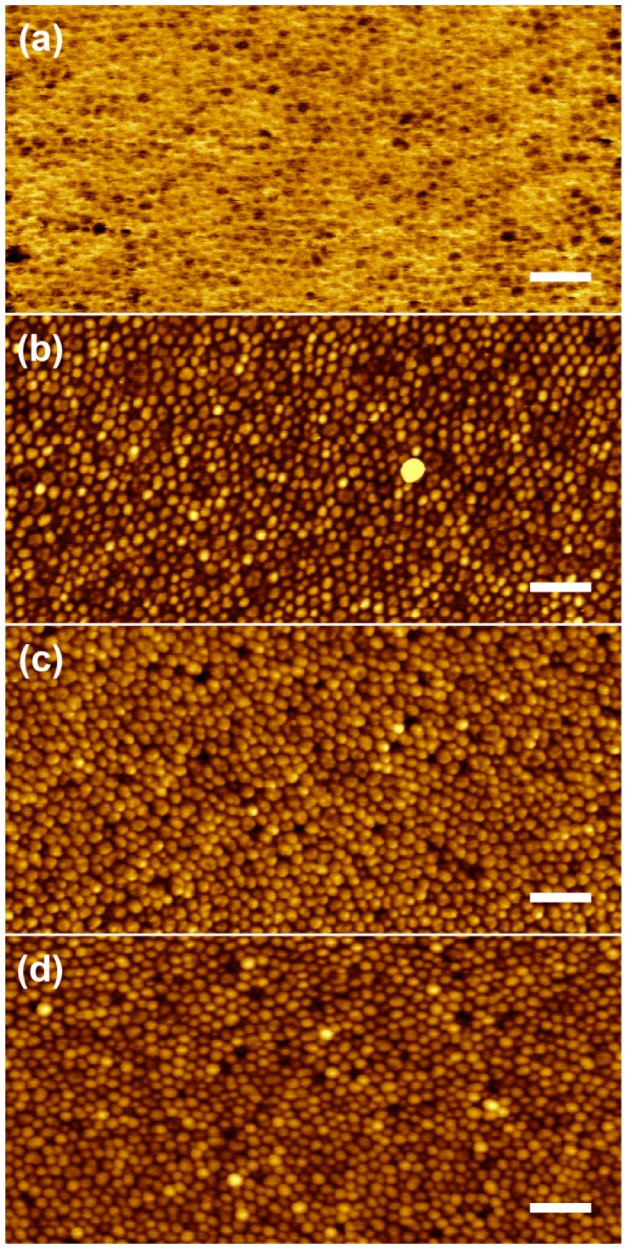

Figure 3. AFM image of the (a) CEO (5.9, 0.42) thin film after a 5 min solvent vapor anneal using a cyclohexane/THF mixture (phase image) and the resulting height images of templated (b) silica, (c) titania, and (d) iron oxide nanoparticles. All images were acquired in tapping mode. Scale bars represent 100 nm.

interactions and lead to an overall reduction of the effective χ of the swollen film.

Annealed and dried films were then impregnated using a simple process of spin-coating alcoholic solutions of inorganic precursors onto the film surface. Through selective interactions and rapid diffusion, these precursors are localized within the PEO domain, whereas the hydrophobic nature of PCHE precludes metal ion inclusion. The organic/inorganic composites were then subjected to UV/O_3 exposure to oxidize the inorganic precursors and degrade the polymer scaffold. Originally developed by Morris et al. using PS-*b*-PEO,[16−18] this versatile procedure templates inorganic nanodot arrays from the metal salt iron nitrate and the sol−gel precursors tetraethyl orthosilicate (TEOS) and titanium ethoxide to produce arrays of iron oxide, silica, and titania nanoparticles, respectively (Figure 3b−d and Figure S13b−d). The procedure employed herein was simplified, and no "activation step", i.e., immersion of the film in ethanol prior to incorporation, was performed. Additional details regarding particle compositions resulting from this generic process are described in the literature.[13,16−18]

The robust nature of the particles was confirmed upon thermal treatment at high temperature (500 °C for 0.5 h); each sample exhibited only a small reduction in the particle size likely due to some sintering (Figure S14). From image analysis, we estimate center-to-center distances and diameters that closely match the initial dimension of the block polymer templates (see Table S4). The heights of the particles range from 1 to 3 nm, depending on the precursor identity. For example, a typical height profile for silica particles obtained from an 18 nm thick polymer film is shown in Figure S15, in which the dot heights vary between 2 and 3 nm. This height reduction of the templated nanodots relative to initial block polymer film thickness is in line with previous work and attributed to the small volume fraction of the metal precursors in the PEO phase.[16−18]

Because the size of the metal oxide dots matches closely the initial diameter of the PEO domains in the previous examples, reduction of the PEO volume fraction and/or overall molar mass can enable the formation of smaller particles. We took advantage of our selective solvent annealing process to organize a very low molar mass sample [CEO (4.1, 0.24), see Table S2]. A thin film of CEO (4.1, 0.24) was annealed in an 80:20 cyclohexane/THF mixture, and small circular features were apparent (Figure S16). Applying the same process to this film, the templated nanoparticle arrays shown in Figure 4 and Figure S17 demonstrate a significant reduction in feature size. Although minor height variations and heterogeneities, ascribed to localized deposition of agglomerated sol−gel precursors and/or potential overfilling of the PEO domains, obscure the overall image clarity, the apparent oxide nanodots formed

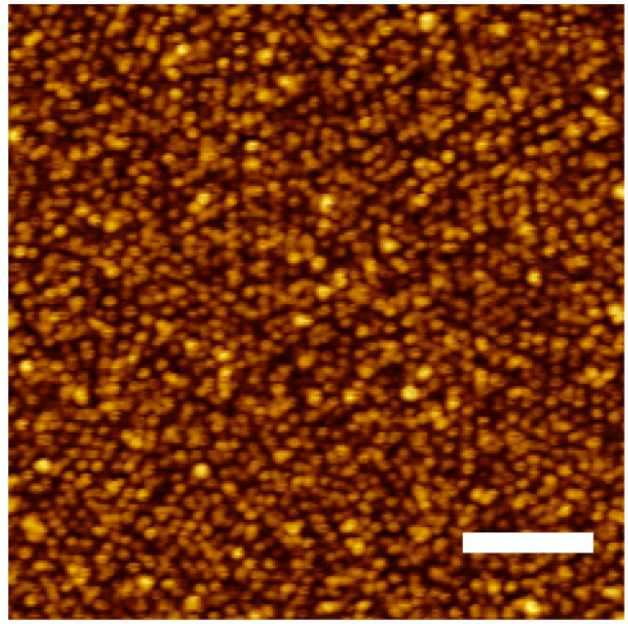

Figure 4. Iron oxide nanoparticles templated from a thin film of CEO (4.1, 0.24). The scale bar represents 100 nm.

DOI: 10.1021/acsmacrolett.5b00458
ACS Macro Lett. 2015, 4, 1027−1032

measure 6 ± 1 nm and represent the smallest particles templated from selective precursor insertion into a block polymer scaffold to date.

In summary, the synthesis of new CEO block polymers by tandem anionic polymerizations and catalytic hydrogenation has been demonstrated. Here, we have illustrated the utility of Si, Ti, and Fe precursors to reproducibly form oxide nanodots on a silicon substrate via a simple and versatile templating process. We have effectively shown a general proof-of-concept for advanced patterning of metal oxides of reduced feature size. Consequently, CEO block polymers represent a valuable system that can be utilized to template a wide breadth of materials through the addition of appropriate inorganic additives. Further work can be done using directed self-assembly for improved long-range order in nanotemplating applications.

■ ASSOCIATED CONTENT

Supporting Information

The Supporting Information is available free of charge on the ACS Publications website at DOI: 10.1021/acsmacrolett.5b00458.

SEC traces of all hydroxyl-terminated precursors and compositionally asymmetric block polymers, precursor and block polymer DSC data, representative ^{1}H NMR spectra, block polymer TGA data, additional AFM images of the block polymer films and the nanoparticle arrays, and a summary of the particle size analysis (PDF)

■ AUTHOR INFORMATION

Corresponding Author

*E-mail: hillmyer@umn.edu.

Notes

The authors declare no competing financial interest.

■ ACKNOWLEDGMENTS

This work was supported primarily by the National Science Foundation through the University of Minnesota MRSEC under Award Number DMR-1420013. Additional support was provided by the Semiconductor Research Corporation. The authors thank Frank Bates, Li Yao, and Justin Kennemur for helpful discussion and Luis Oquendo and Chris Fretham for SEM imaging. CS thanks the University of Minnesota for partial support during his sabbatical leave. The CNRS and the Université d'Orléans are acknowledged for support. Portions of this work were performed at the Advanced Photon Source (APS), Sector 5 (DuPont-Northwestern-Dow Collaborative Access Team, DND-CAT) and Sector 12. DND-CAT is supported by Northwestern University, E.I. DuPont de Nemours & Co., and The Dow Chemical Company. This research used resources of the Advanced Photon Source, a U.S. Department of Energy (DOE) Office of Science User Facility operated for the DOE Office of Science by Argonne National Laboratory under Contract No. DE-AC02-06CH11357. Parts of this work were carried out in the College of Science and Engineering Characterization Facility, University of Minnesota, which receives partial support from NSF through the MRSEC program.

■ REFERENCES

(1) Wang, X.; Li, Z.; Shi, J.; Yu, Y. *Chem. Rev.* **2014**, *114*, 9346−9384.
(2) Cui, Y.; Björk, M. T.; Liddle, J. A.; Sönnichsen, C.; Boussert, B.; Alivisatos, A. P. *Nano Lett.* **2004**, *4*, 1093−1098.
(3) Baruth, A.; Rodwogin, M. D.; Shankar, A.; Erickson, M. J.; Hillmyer, M. A.; Leighton, C. *ACS Appl. Mater. Interfaces* **2011**, *3*, 3472−3481.
(4) Park, S.; Lee, D. H.; Xu, J.; Kim, B.; Hong, S. W.; Jeong, U.; Xu, T.; Russell, T. P. *Science* **2009**, *323*, 1030−1033.
(5) Peng, J.; Li, X.; Kim, D. H.; Knoll, W. *Macromol. Rapid Commun.* **2007**, *28*, 2055−2061.
(6) Li, Y.; Sasaki, T.; Shimizu, Y.; Koshizaki, N. *J. Am. Chem. Soc.* **2008**, *130*, 14755−14762.
(7) Gu, X.; Gunkel, I.; Russell, T. P. *Philos. Trans. R. Soc. A* **2013**, *371*.
(8) Bang, J.; Jeong, U.; Ryu, D. Y.; Russell, T. P.; Hawker, C. J. *Adv. Mater.* **2009**, *21*, 4769−4792.
(9) Bates, C. M.; Maher, M. J.; Janes, D. W.; Ellison, C. J.; Willson, C. G. *Macromolecules* **2013**, *47*, 2−12.
(10) Nunns, A.; Gwyther, J.; Manners, I. *Polymer* **2013**, *54*, 1269−1284.
(11) Chai, J.; Buriak, J. M. *ACS Nano* **2008**, *2*, 489−501.
(12) Sweat, D. P.; Kim, M.; Larson, S. R.; Choi, J. W.; Choo, Y.; Osuji, C. O.; Gopalan, P. *Macromolecules* **2014**, *47*, 6687−6696.
(13) Roulet, M.; Vayer, M.; Sinturel, C. *Eur. Polym. J.* **2013**, *49*, 3897−3903.
(14) Chinthamanipeta, P. S.; Lou, Q.; Shipp, D. A. *ACS Nano* **2011**, *5*, 450−456.
(15) Chaudhari, A.; Ghoshal, T.; Shaw, M. T.; Cummins, C.; Borah, D.; Holmes, J. D.; Morris, M. A. *Proc. SPIE* **2014**, 905110.
(16) Mayeda, M. K.; Hayat, J.; Epps, T. H.; Lauterbach, J. *J. Mater. Chem. A* **2015**, *3*, 7822−7829.
(17) Ghoshal, T.; Maity, T.; Godsell, J. F.; Roy, S.; Morris, M. A. *Adv. Mater.* **2012**, *24*, 2390−2397.
(18) Ghoshal, T.; Shaw, M. T.; Bolger, C. T.; Holmes, J. D.; Morris, M. A. *J. Mater. Chem.* **2012**, *22*, 12083−12089.
(19) Kim, D. H.; Kim, S. H.; Lavery, K.; Russell, T. P. *Nano Lett.* **2004**, *4*, 1841−1844.
(20) Varghese, J.; Ghoshal, T.; Deepak, N.; O'Regan, C.; Whatmore, R. W.; Morris, M. A.; Holmes, J. D. *Chem. Mater.* **2013**, *25*, 1458−1463.
(21) Hillmyer, M. A.; Bates, F. S. *Macromolecules* **1996**, *29*, 6994−7002.
(22) Hillmyer, M. A.; Bates, F. S.; Almdal, K.; Mortensen, K.; Ryan, A. J.; Fairclough, J. P. A. *Science* **1996**, *271*, 976−978.
(23) Hajduk, D. A.; Takenouchi, H.; Hillmyer, M. A.; Bates, F. S.; Vigild, M. E.; Almdal, K. *Macromolecules* **1997**, *30*, 3788−3795.
(24) Cochran, E. W.; Bates, F. S. *Macromolecules* **2002**, *35*, 7368−7374.
(25) Gehlsen, M. D.; Bates, F. S. *Macromolecules* **1993**, *26*, 4122−4127.
(26) Kennemur, J. G.; Yao, L.; Bates, F. S.; Hillmyer, M. A. *Macromolecules* **2014**, *47*, 1411−1418.
(27) Wolf, J. H.; Hillmyer, M. A. *Langmuir* **2003**, *19*, 6553−6560.
(28) Hillmyer, M. A.; Bates, F. S. *Macromol. Symp.* **1997**, *117*, 121−130.
(29) Zhu, L.; Cheng, S. Z. D.; Calhoun, B. H.; Ge, Q.; Quirk, R. P.; Thomas, E. L.; Hsiao, B. S.; Yeh, F.; Lotz, B. *Polymer* **2001**, *42*, 5829−5839.
(30) Loo, Y.-L.; Register, R. A.; Ryan, A. J. *Macromolecules* **2002**, *35*, 2365−2374.
(31) Lee, S.; Gillard, T. M.; Bates, F. S. *AIChE J.* **2013**, *59*, 3502−3513.
(32) Gillard, T. M.; Medapuram, P.; Morse, D. C.; Bates, F. S. *Macromolecules* **2015**, *48*, 2801−2811.
(33) Matsen, M. W. *Macromolecules* **2012**, *45*, 2161−2165.
(34) Matsen, M. W.; Bates, F. S. *J. Polym. Sci., Part B: Polym. Phys.* **1997**, *35*, 945−952.
(35) Lynd, N. A.; Hillmyer, M. A.; Matsen, M. W. *Macromolecules* **2008**, *41*, 4531−4533.
(36) Cooke, D. M.; Shi, A.-C. *Macromolecules* **2006**, *39*, 6661−6671.

DOI: 10.1021/acsmacrolett.5b00458
ACS Macro Lett. 2015, 4, 1027−1032

(37) Cochran, E. W.; Morse, D. C.; Bates, F. S. *Macromolecules* **2003**, *36*, 782−792.
(38) Phillip, W. A.; Hillmyer, M. A.; Cussler, E. L. *Macromolecules* **2010**, *43*, 7763−7770.
(39) Sinturel, C.; Vayer, M.; Morris, M.; Hillmyer, M. A. *Macromolecules* **2013**, *46*, 5399−5415.
(40) Ellison, C. J.; Cushen, J. D.; Willson, C. G. *J. Photopolym. Sci. Technol.* **2013**, *26*, 45−47.
(41) Cushen, J. D.; Wan, L.; Pandav, G.; Mitra, I.; Stein, G. E.; Ganesan, V.; Ruiz, R.; Willson, C. G.; Ellison, C. J. *J. Polym. Sci., Part B: Polym. Phys.* **2014**, *52*, 36−45.
(42) Wu, H. S.; Sandler, S. I. *J. Chem. Eng. Data* **1988**, *33*, 157−162.
(43) Sinturel, C.; Bates, F. S.; Hillmyer, M. A. *ACS Macro Lett.*, 2015, in press.

DOI: 10.1021/acsmacrolett.5b00458
ACS Macro Lett. 2015, 4, 1027−1032